Supporting information for

Van der Waals integration of AZO/MoS_2 ohmic junctions toward high-performance transparent 2D electronics

Tao Guo,[a] Hao Wu,[b,*] Xue Chen,[a] Qi Tang,[a] Jiaxian Wan,[a] Quanbing Guo,[a] Shuangfeng Jia,[a] and Chang Liu[a,*]

[a] Key Laboratory of Artificial Micro- and Nano-structures of Ministry of Education, and School of Physics and Technology, Wuhan University, Wuhan 430072, China;

[b] Hubei Nuclear Solid Physics Key Laboratory, and School of Physics and Technology, Wuhan University, Wuhan 430072, China.

[*]Authors to whom any correspondence should be addressed

E-mail: h.wu@whu.edu.cn and chang.liu@whu.edu.cn

Figure S1

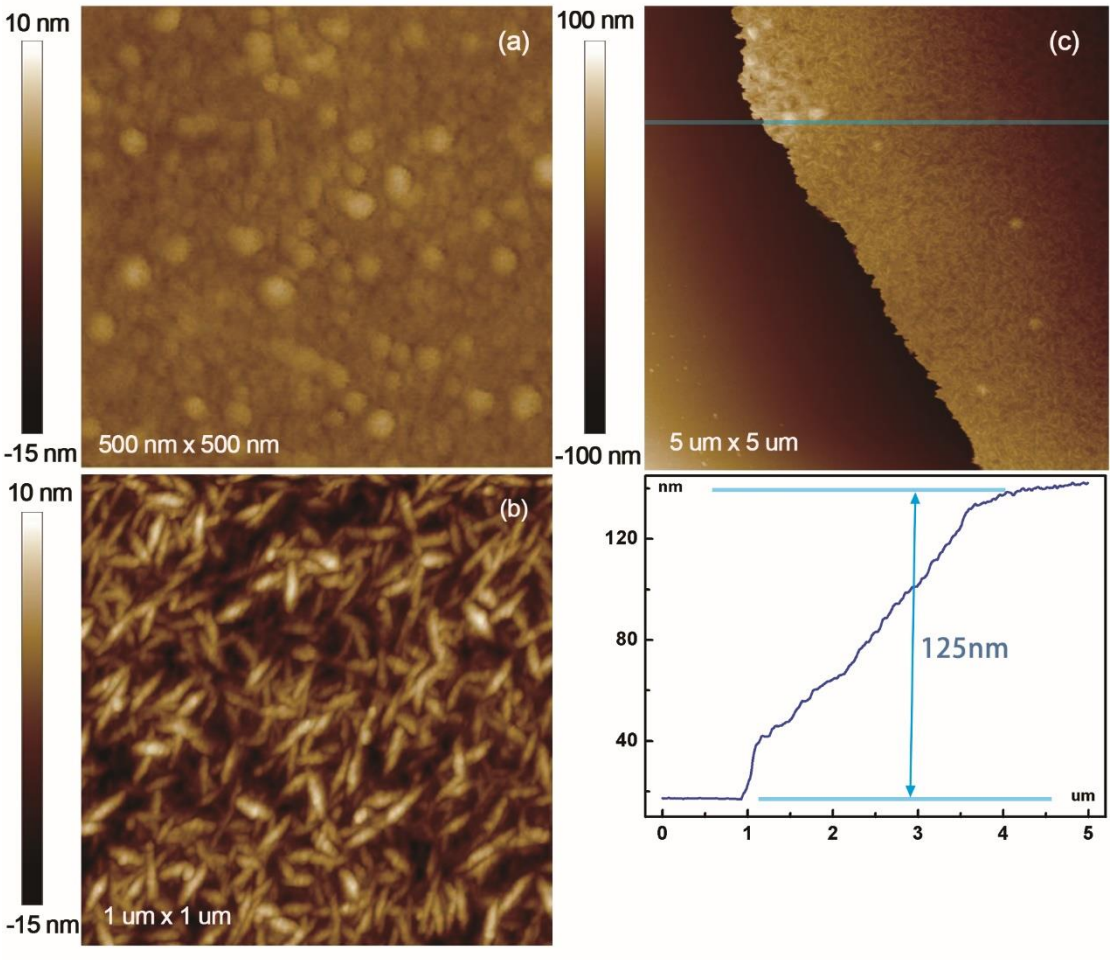

Figure S1. AFM images of (a) 20 nm thick ZnO thin films and (b) 125 nm thick AZO thin films on MoS_2. (c) The film step of AZO on MoS_2 scanned by AFM.

To further confirm that the dense and continuous thin films can be gained by atomic layer deposition (ALD) on dangling bonds-free MoS_2 surface, 20 nm thick ZnO thin films were grown on MoS_2 with optimal H_2O treatment cycles. Its surface morphologies are shown in **Fig. S1**(a) by atomic force microscope (AFM) measurements. The small grains are clearly observed and get together to form the consecutive films, implying that high-quality films on 2D materials can be obtained

by ALD using this treatment method. In this way, 125 nm thick AZO thin films were grown MoS_2, the AFM image of those is shown in **Fig S1**(b). One can notice that the dense and consecutive AZO thin films have been obtained and the shape of small grain becomes to be taper due to the doped-Al in ZnO. In order to measure the actual film thickness of AZO thin films on MoS_2, the film step was prepared by photolithography and chemical etching. **Figure S1**(c) shows that the thickness of AZO thin films is approximately 125 nm, which is in agreement with the designed ALD cycles with growth rate of 4.1 nm. The sheet resistance of 125 nm thick AZO thin films is about 400 Ω/□, tested by Hall-effect measurements.

Figure S2

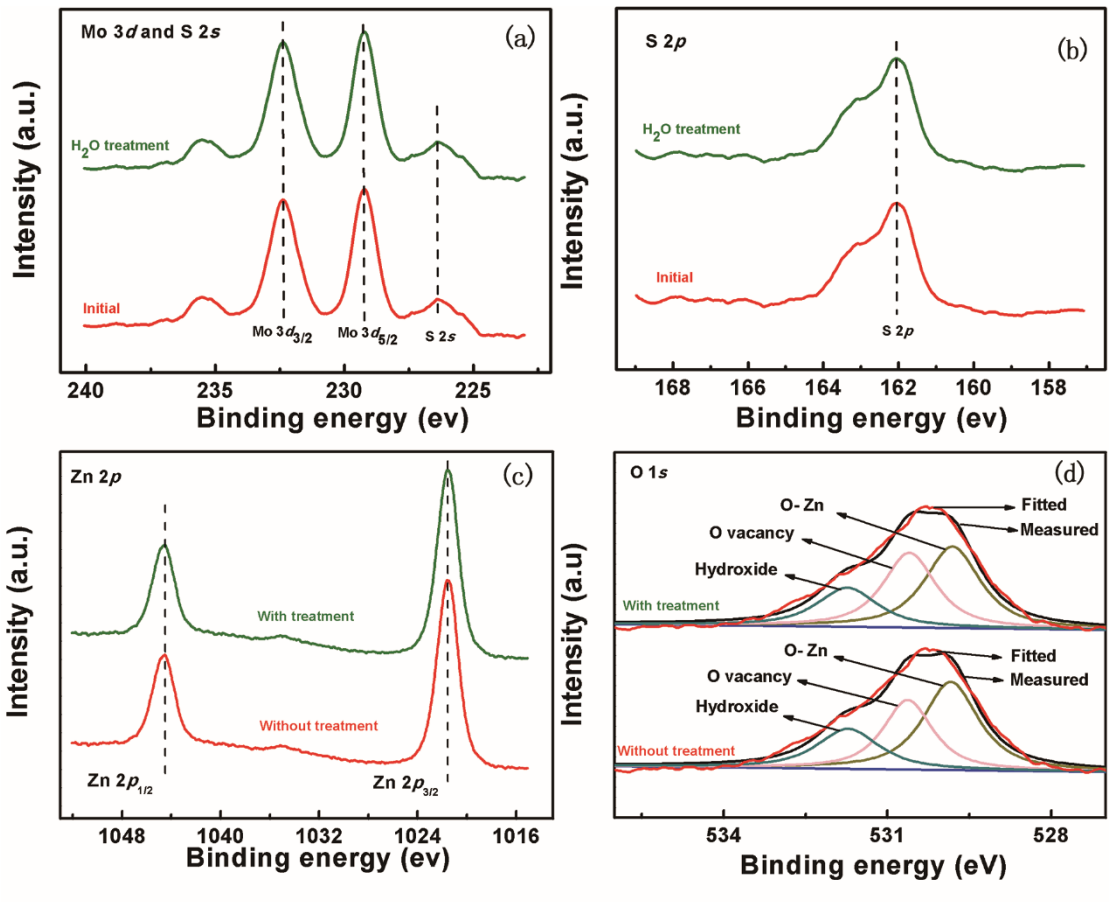

Figure S2. XPS spectra of (a) Mo 3d, S 2s and (b) S 2p core level peaks for monolayer MoS_2 films, (c) Zn 2p and (d) O 1s core level peaks for ALD-grown ZnO thin films with and without H_2O treatments.

The bonding characteristics and stoichiometry of MoS_2 and ALD-grown ZnO thin films on MoS_2 with and without H_2O treatments are investigated by X-ray photoelectron spectroscopy (XPS) as well. For the initial MoS_2, Mo 3d doublet peaks and S 2_S peaks, located at about 232.6 eV, 229.4 eV and 226.9 eV, respectively, [1-2] are distinctly presented in **Fig. S2**(a). In the S 2p core level spectra, the peak is observed at 162.1 eV in **Fig. S2**(b). After with H_2O treatments, the characteristic peaks of Mo

and S atom are nearly identical, as presented in **Fig. S2**(a) and (b), respectively. Moreover, The calculated stoichiometric ratio (S/Mo) is 1.98, which is consistent with those before H_2O treatments. These results suggest that the process of H_2O treatments did not change the stoichiometry relationships between S and Mo atom or introduced any defects into MoS_2. **Figure S2**(c) shows the Zn 2p core level spectra of ALD-grown ZnO thin films on MoS_2. For that with H_2O treatments, the characteristic binding energies of Zn $2p_{1/2}$ and Zn $2p_{3/2}$ are obtained at 1044.6 and 1021.6 ev, respectively. [3-4] The same results are observed for that without H_2O treatments. The O 1s core level spectra of ZnO, as shown in **Fig. S2**(d), are divided as three typical separated peaks by Gaussian fitting with the subtraction of a Shirley type background, corresponding to O-Zn with a low binding energy (530.3 eV), O vacancy with a middle binding energy (530.7 eV), and hydroxide (such as O-H and O-C group) with a high binding energy (532.1 eV), respectively. The binding energies of the three peaks in O 1s core level spectra are located at the same point in horizontal axis for the ZnO with and without H_2O treatments, related to the fact that the adsorbed H_2O on the MoS_2 surface almost have no influence on the bonding type of ALD-grown ZnO. Hence, the XPS results demonstrate that the process of H_2O treatments almost has no impact on MoS_2 and the followed ALD-grown ZnO thin films.

Figure S3

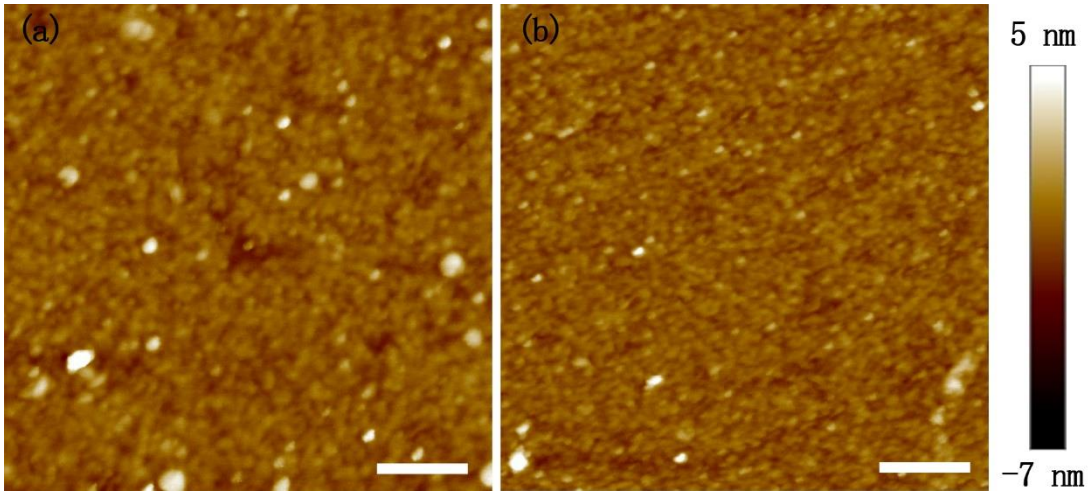

Figure S3. AFM images of ZnO on graphene (a) without and (b) with H_2O treatments on graphene. Scale bar: 200 nm.

Figure S3 shows the surface morphologies of ZnO thin films on graphene without and with vdWs epitaxy of buffer layer. For that without H_2O treatments, many dark holes exist on the graphene surface without the coverage of ZnO thin films, as shown in **Fig. S3**(a), implying the insufficient nucleation sites for the ALD growth. When introduction of H_2O treatments on graphene, the ZnO thin films can continuously grow and the defects of dark holes are hardly seen on the surface in the optimal treatment condition, as shown in **Fig. S3**(b). The similar ohmic behavior was observed in the AZO-graphene junctions by creation of vdWs junctions, as shown in

Figure S4

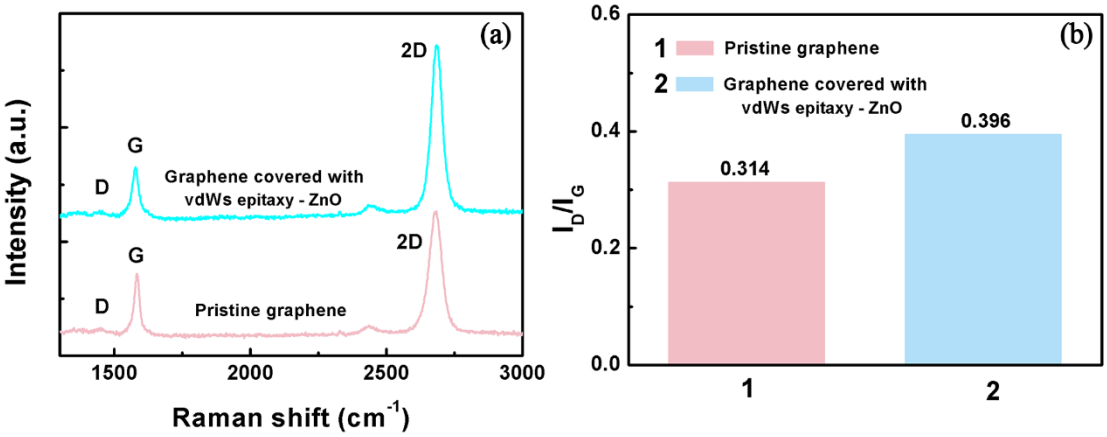

Figure S4. (a) Raman spectra and (b) the ratio of I_D/I_G of pristine graphene and graphene covered with vdWs epitaxy - ZnO.

Figure S4(a) shows three typical Raman peaks (D, G, 2D) of the pristine graphene and graphene covered by the vdWs epitaxy - ZnO films.[5] Pristine graphene presents distinct G and 2D peaks at ~1600 and ~2700 cm^{-1}, respectively. The D peak could be observed in the pristine graphene at 1350 cm^{-1}, which was related to the defects in graphene, and indicated that the defects of the CVD-grown pristine graphene could not be ignored.[6] The ratio of the peak intensities between D and G (I_D/I_G) clearly reflected the defect density of graphene.[7] Figure **S4**(b) shows the I_D/I_G ratios of graphene, which were almost unchanged after covering with vdWs epitaxy -ZnO films compared to that of the pristine graphene, implying that the vdWs epitaxy process of ZnO films did not introduce noticeable defects into the graphene.

Figure S5

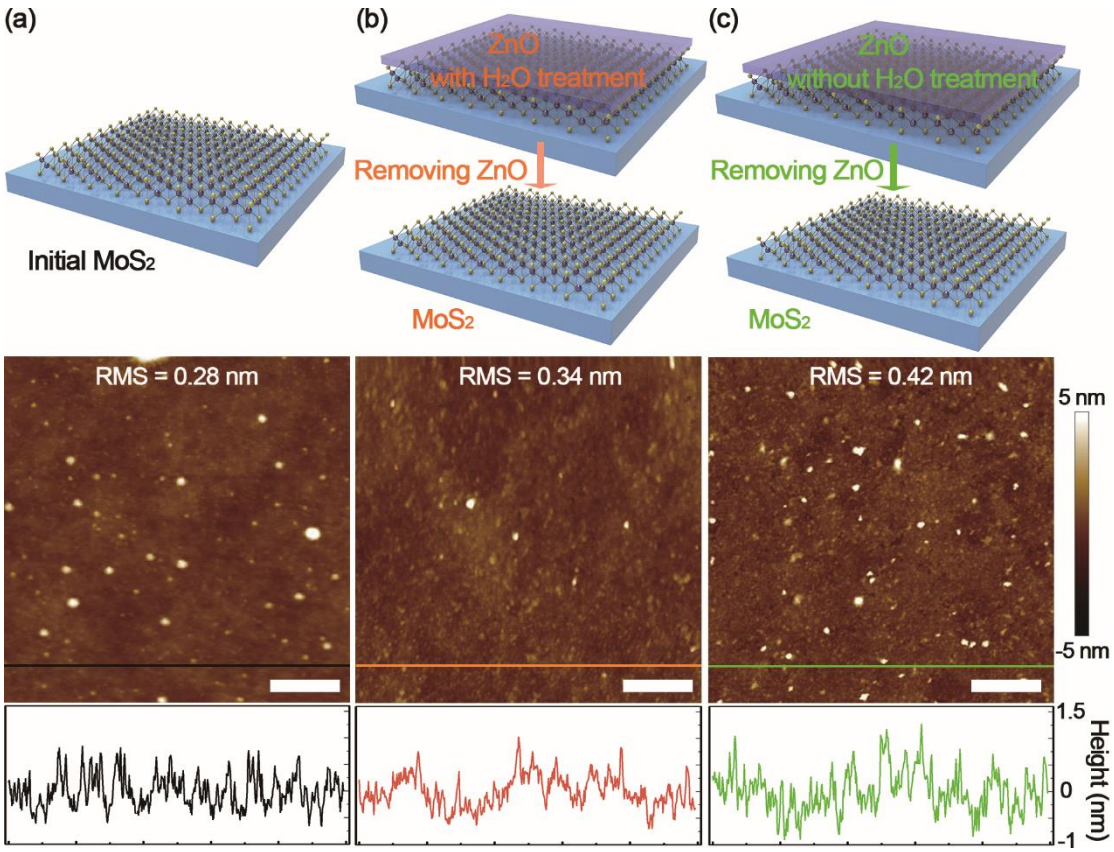

Figure S5. AFM images of MoS_2 surfaces: (a) initial, (b) with and (c) without H_2O treatment after removing ZnO buffer layer. Scale bar: 200 nm.

To demonstrate the weak vdWs interaction at the interface, we removed the ZnO buffer layer from MoS_2 after the ALD growth and compared the underlying MoS_2 with the initially virgin MoS_2 . **Figure S5**(a) shows the AFM image of the initial MoS_2 film with a RMS roughness of 0.27 nm. After depositing ZnO thin films on MoS_2 with H_2O treatments, no detectable defects can be found on the surface and the RMS just increases a little to 0.34 nm, as presented in **Fig. S5**(b). In contrast, for ZnO on MoS_2 that is not treated by H_2O, the black pinhole defects occur, and the RMS roughness increases up to 0.44 nm, as seen in **Fig. S5**(c). As a result, the successful

integration of AZO–MoS_2 junctions by the vdWs force strongly suggests ideal interfaces between two materials that are in intimate contact keeping their isolated states without any direct chemical reactions.

Figure S6

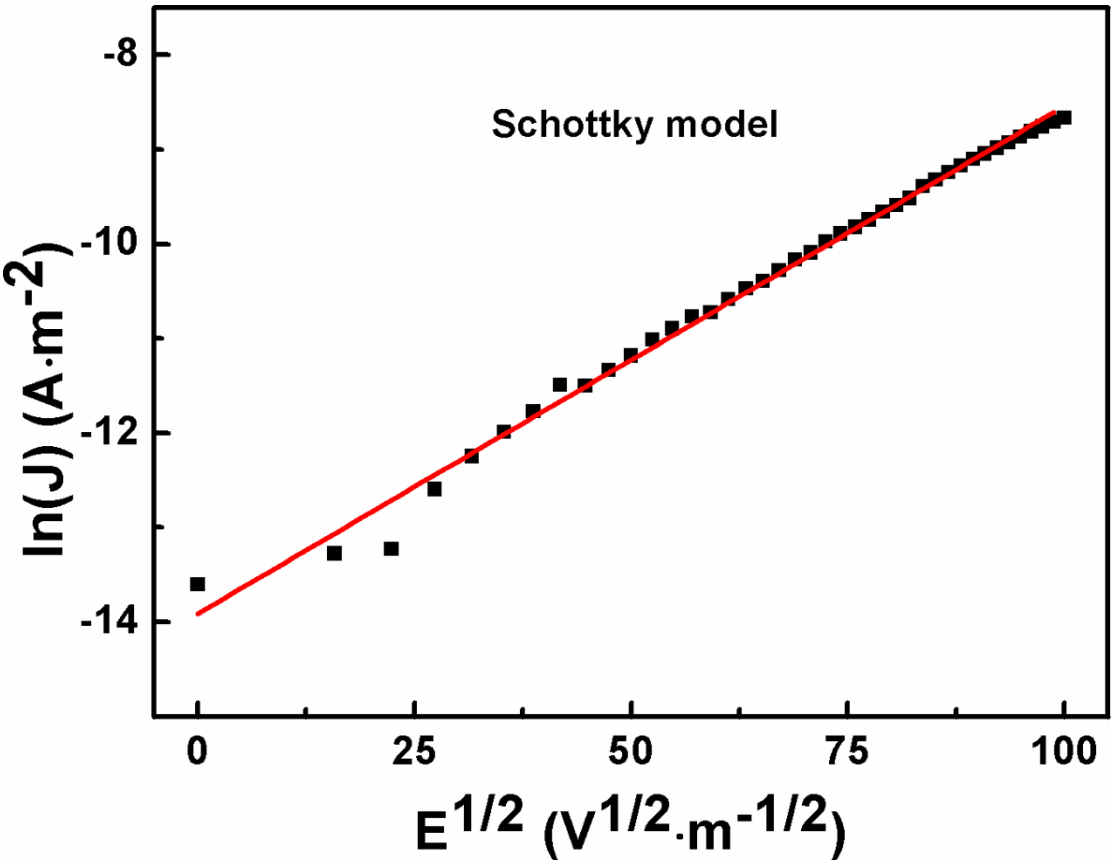

Figure S6. The leakage current mechanism of Schottky emission.

Figure S7

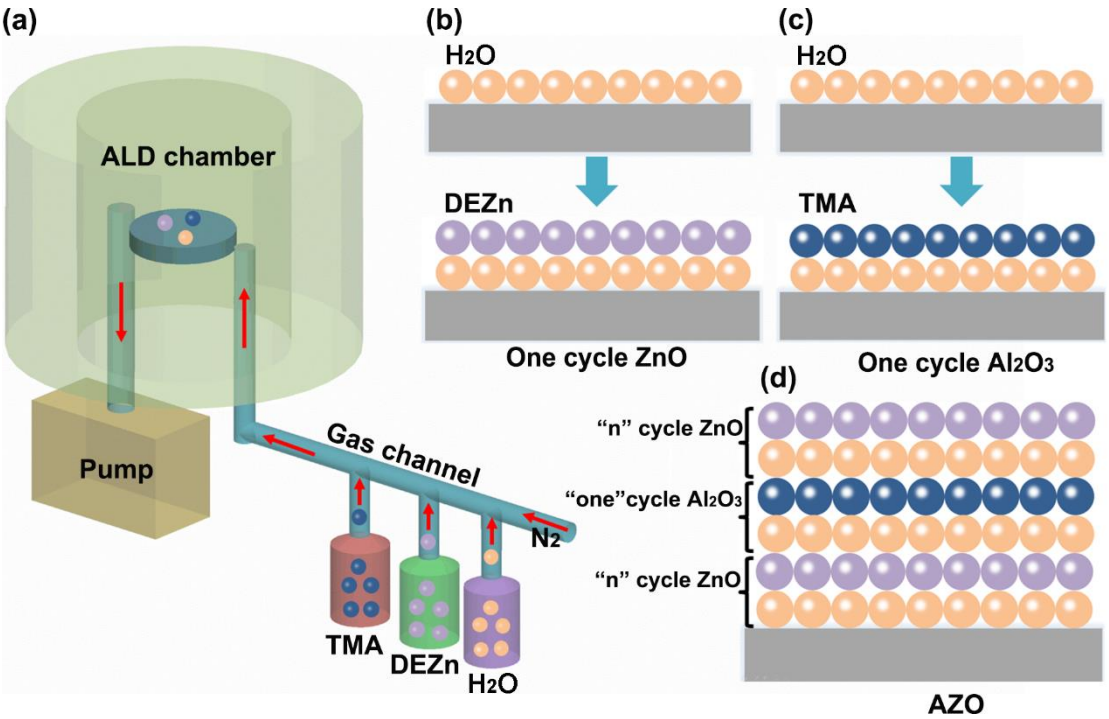

Figure S7. Schematic of the ALD process and AZO film growth. (a) ALD setup for the depositions; atomic schematic of the ALD (b) DEZn and (c) TMA precursor cycles; (d) illustration of the precursor pulse sequences employed to grow the AZO films by ALD.

Figure S7 shows the schematic of the ALD process and AZO film growth. "one" layer of AZO thin films contains "n" layers ZnO thin films, "one" layer Al_2O_3 thin films and another "n" layers ZnO thin films, respectively.

Figure S8

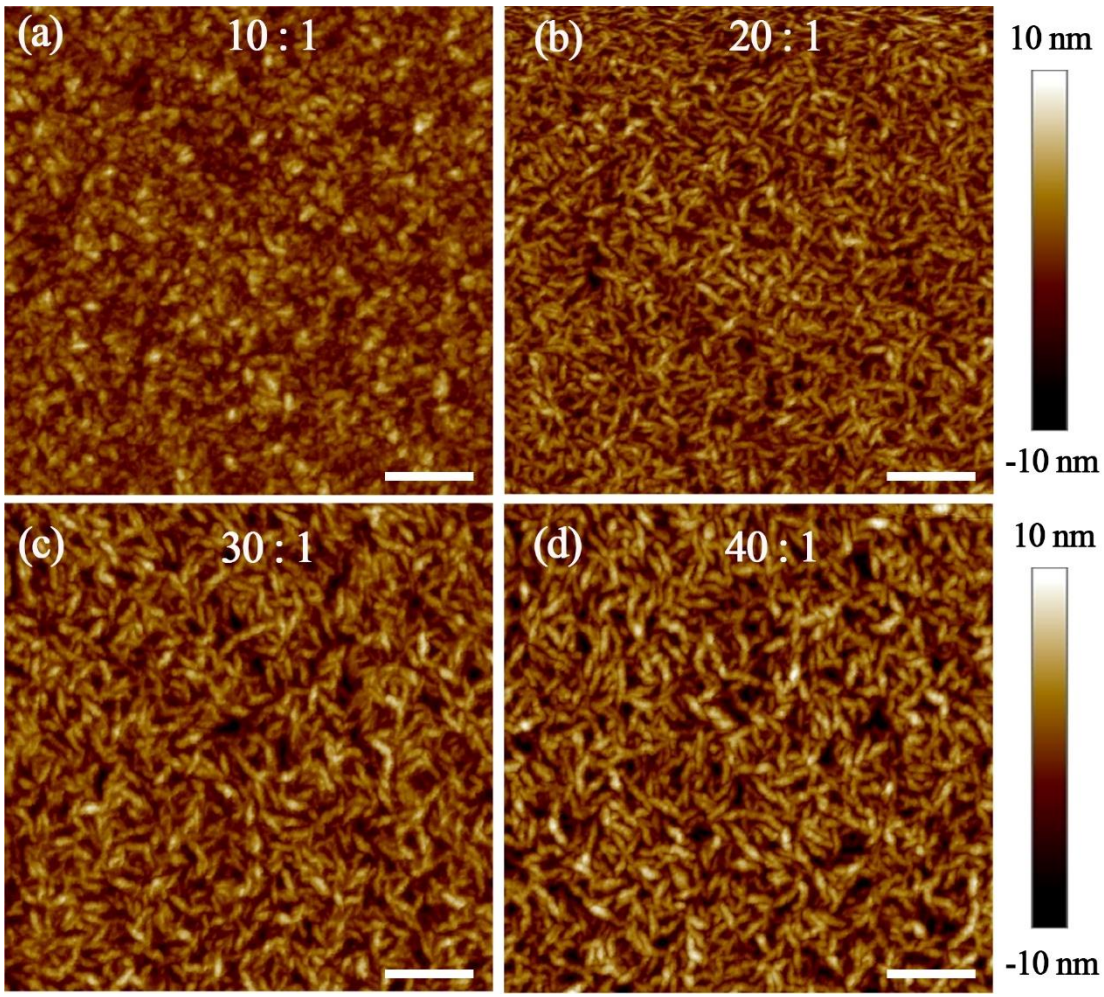

Figure S8. The surface morphologies of AZO thin films with different Zn:Al precursor ratio: (a) 10:1, (b) 20:1, (c) 30:1, (d) 40:1. Scale bar: 200 nm.

Figure S9

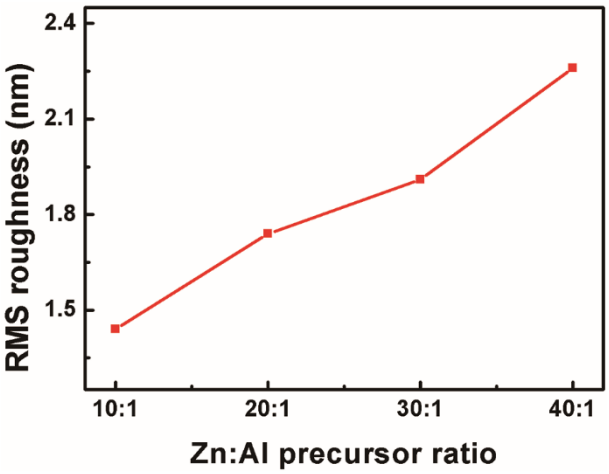

Figure S9. The RMS roughness of AZO thin films with different Zn:Al precursor ratio.

Figure S10

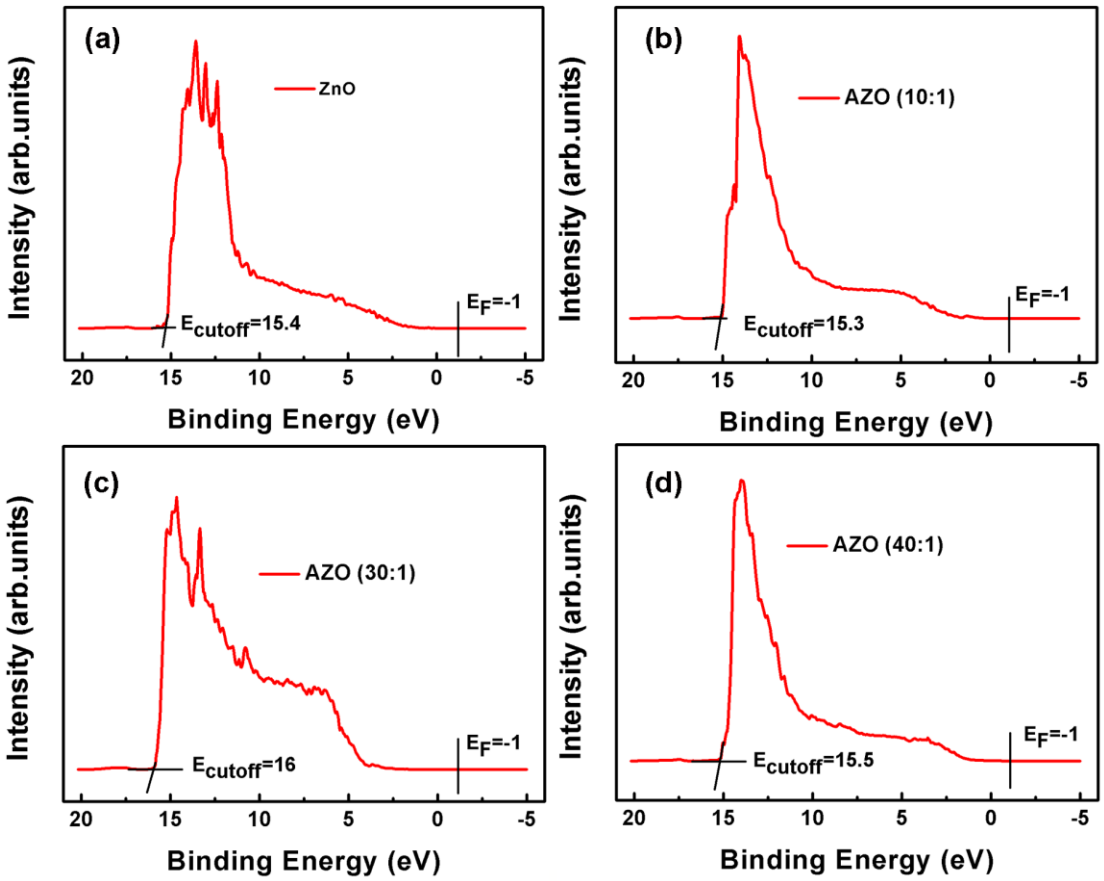

Figure S10. UPS spectra of ZnO and AZO with different Zn:Al precursor ratio

The ultraviolet photoelectron spectroscopy (UPS) spectra were measured to calculate the work function (WF) of ZnO, AZO and MoS_2. Here, The UPS spectra were recorded using a *He* I radiation ($h\nu$ = 21.22 eV) from an unfiltered gas discharge lamp with step size of 0.025 eV. The WF can be obtained by the following formula: [8]

$$WF = h\nu - (E_{cutoff} - E_F)$$

Where E_{cutoff} and E_F are the energy of secondary electron cutoff and Fermi level, respectively. Figure S6 shows the UPS spectra of ZnO and AZO with different Zn:Al precursor ratio. To trade off the performance of conductance and work function, the Zn:Al precursor ratio is set as 20:1 in this work.

Figure S11

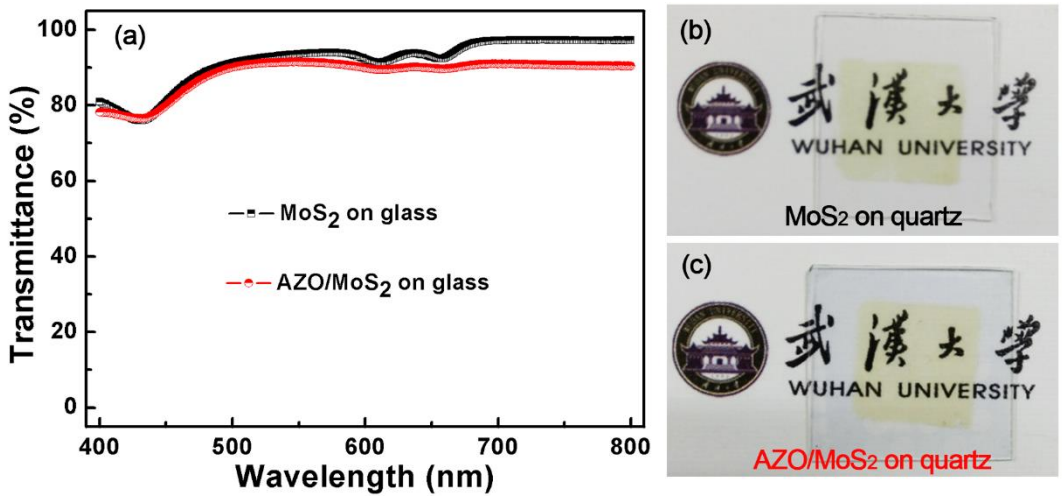

Figure S11. (a) Transmittance spectra of MoS_2 and AZO on MoS_2. The actual picture of (b) MoS_2 and (c) AZO on MoS_2.

Figure S12

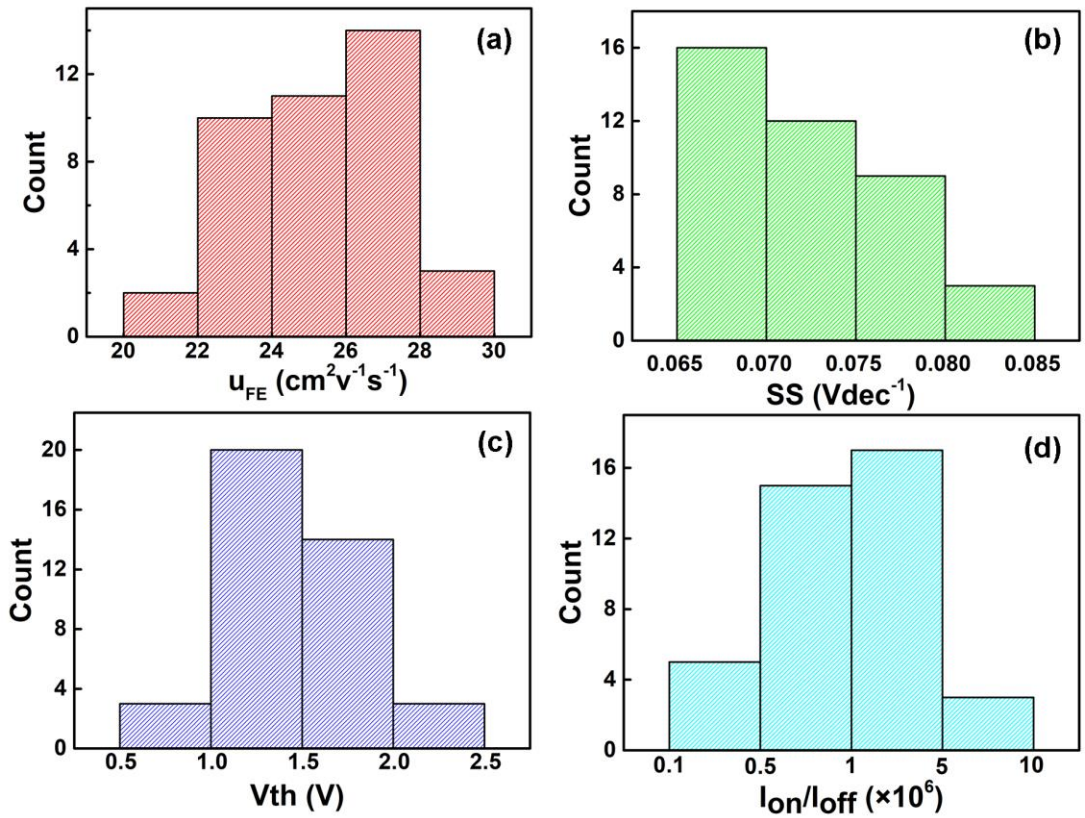

Figure S12. Distribution of the values of μ_{FE}, SS, Vth and Ion/Ioff measured from 40 different transparent TFTs.

■ Reference

1 N. Liu, P. Kim, J. H. Kim, J. H. Ye, S. Kim, C. J. Lee, *ACS NANO*, 2014, **8**, 6902-6910.

2 H. Dong, C. Gong, R. Addou, S. McDonnell, A. Azcatl, X. Qin, W. Wang, W. Wang, C. L. Hinkle, R. M. Wallace, *ACS APPL MATER INTER*, 2017, **9**, 38977-38983.

3 C. Yu, K. Yang, Y. Xie, Q. Fan, J. C. Yu, Q. Shu, C. Wang, *NANOSCALE*, 2013, **5**, 2142.

4 C. WOLL, *PROG SURF SCI*, 2007, **82**, 55-120.

5 Y. H. Park, M. H. Kim, S. B. Kim, H. J. Jung, K. Chae, Y. H. Ahn, J. Park, F. Rotermund, S. W. Lee, *CHEM MATER*, 2016, **28**, 7268-7275.

6 Y. Yamada, K. Murota, R. Fujita, J. Kim, A. Watanabe, M. Nakamura, S. Sato, K. Hata, P. Ercius, J. Ciston, C. Y. Song, K. Kim, W. Regan, W. Gannett, A. Zettl, *J AM CHEM SOC*, 2014, **136**, 2232-2235.

7 J. C. M. V. A. C. Ferrari, S. R. A. A. K. S. Novoselov, *PHYS REV LETT*, 2006, 187401.

8 W. Wang, Q. Feng, K. Jiang, J. Huang, X. Zhang, W. Song, R. Tan, *APPL SURF SCI*, 2011, **257**, 3884-3887.